Robotica (2004) volume 22, pp. 271–283. © 2004 Cambridge University Press
DOI: 10.1017/S0263574703005599 Printed in the United Kingdom

Dynamic control of multi-arm co-operating manipulator systems

Anjan Kumar Swain* and Alan S. Morris†

(Received in Final Form: September 10, 2003)

SUMMARY

This paper deseribes the control of multi-arm co-operating manipulator systems handling a common object. Inverse dynamics controllers with motive force compensation are developed for the co-operating fixed-base, free-floating, and free-flying space manipulator systems. Further, the relative performances of all the three configurations are compared on two tracking problems.

KEYWORDS: Fixed-base; Free-floating; Free-flying; Space manipulators.

1. INTRODUCTION

One of the most important and increasingly popular areas of robotic systems research is the co-operative robotic system. This is because of the capability of co-operating manipulators to handle more difficult jobs that cannot be easily handled by a single manipulator. These jobs include handling large, heavy or non-rigid objects; mating of mechanical parts; and space robotic applications. The potential of these systems can only be achieved through an efficient co-ordination control strategy. However, the control and analysis of co-ordinated systems to maintain any desired co-operation are much more complex due to the presence of inherent kinematic and dynamic interactions. In addition, a set of closed kinematic chains is formed when the object is held rigidly by a number of manipulators. Further, when the contact surface is rigid, then the contact force is a constraint reaction. Then, for this constrained system with reduced degrees of freedom, the contact force can only be controlled by directly controlling the actuator torques.[1] Then, this condition imparts sundry kinematic and dynamic constraints on manipulator position, velocity and acceleration. Thus, a co-operative manipulator system cannot be controlled independently to meet given tracking criteria. This is mainly due to the fact that an individual controller associated with a particular manipulator would respond to its own tracking errors regardless of the actions of the other manipulators, thereby leading to the reduced life span of components, parts damaging, and the satellite tumbling out of control in space, etc.

Co-operative arm control methods broadly fall into three categories:[2] (i) the master-slave control,[3–7] (ii) the hybrid position/force control[8,9] and (iii) the dynamic co-operation method.[10–12] In the master-slave method, the master arm is position controlled and the slave arm follows the master with a force feedback. Thc major problem associated with this method is that the impedance of the slave arm must be very small to exactly follow the motion of the master arm. Further, it is not clear how the torque will be distributed optimally among the arms during task execution. Due to these reasons, the master-slave method is not effective at all for co-operative control.[9,13]

The hybrid position/force control method of Raibert and Craig[14] was extended by Hayati[8,15] to multi-arm co-operating robots. In this control method, the extra degrees of freedom of the multiple manipulator system are used to control the internal force. This hybrid control method has been criticised as being fundamentally flawed. A critical analysis with a historical perspective on hybrid control methods can be found in Vukobratovic and Stojic.[17]

Dynamic co-operation strategies take into account both manipulator and object dynamics and use a computed torque control algorithm to achieve the desired task. Computed torque control-based approaches have the advantage of being extended easily to various different types of contact such as sliding, rolling etc.[18,19] Luecke and Lai[20] presented a joint error controller for multiple manipulators. In this work, the internal force is cancelled by modifying the trajectory specification by an amount proportional to the internal force. Wen and Kreutz[21,22] independently developed a decoupled control approach for multiple manipulators. Caccavale *et al.*[23] have described a task-space regulation scheme for a dual manipulator system tightly grasping a rigid object. The regulator is based on kinetostatic filtering of the control action and internal force feedback.

A few numbers of publications are available on multiple-arm space manipulator systems. Murphy *et al.*[24] implemented the control algorithm of Rodriguez[25] control a dual-arm co-operating manipulator system handling a common object such that the centre of mass of the object achieves a point-to-point motion control. However, they have reported that the integration error amplifies the error in the tip forces, which in turn leads to instability by violating the kinematic constraint due to the closed chain. They have suggested a possible method to overcome this problem by choosing one arm to be a reference arm and then calculating the velocities of the other arm from that of the reference arm. Then, these velocities are integrated to yield the actual joint angles. However, it is not clear how their proposition is going to avoid this instability, because this particular constraint on end-effector velocities is already included in the controller development phase. Apart from this, they have also not simulated any internal force controllers. Yokoji *et al.*[26] developed an efficient resolved acceleration control

* Department of Electrical Engineering, Indira Gandhi Institute of Technology, Sarang, India.
† Department of Automatic Control and Systems Engineering, University of Sheffield, UK. E-mail: swainanjan@hotmail.com, a.morris@sheffield.ac.uk

algorithm for the generalized Jacobian matrix of a multi-arm space manipulator system. They have shown that the computational complexity of resolved acceleration control and generalised Jacobian are two and five times greater than that of their fixed-base counterpart, respectively. Papadopoulos and Moosavian[27] described the kinematics and dynamics of multi-arm manipulators using body-fixed barycentric vectors, and simulated that for target chasing and capture operations in space. They advocated a structurally simple transpose Jacobian control method because of its simplicity and reduced computational burden compared to model-based control algorithms. Yale and Agrawal[28] discussed repositioning of an object rigidly grasped by space free-floating manipulators. They used a polynomial reference trajectory and reported good control performance. Hu and Vucovich[29] used the concepts of Murphy *et al.*[24] to control a multi-arm free-floating space manipulator system handling an object. They also used momentum conservation and an inertially fixed system centre of mass to represent spacecraft velocity in terms of the actively controlled joint velocities. However, the incorporation of these features rather restricts the workspace and increases the dynamic singularity problems. In addition, the momentum conservation does not hold good when the manipulator end-effectors are in contact with some surface. Thus, it severely restricts the generality of any modelling and control philosophy. They implemented a computed torque like, hybrid position/force controller to track a desired trajectory of the centre of mass of the object.

It can be observed from above that multiple co-operating manipulators are independently studied, particularly for fixed base and free-floating space manipulator systems. However, no detailed work appears to have been carried out on the multi-arm, co-operating, space, free-flying systems. Moreover, no studies have been reported on the behaviour of all the different manipulator systems in an integrated environment. Therefore, in this paper, in addition to the development of the control algorithms for fixed-base, free-floating and free-flying systems, broadly two aspects of co-operating manipulator systems have been studied. Firstly, independent behaviour of all the three configurations is analysed to solve a particular task. Secondly, an integrated analysis of all these manipulator systems is presented to solve different tasks.

The major goal of this paper is to design, develop and analyse control algorithms for fixed base, free-floating and free-flying space manipulator systems to deal with the same task but in different environments. Further, the aim is to compare the relative performances of the three different manipulator configurations, with particular emphasis on space manipulation tasks.

To achieve the desired goal set for this paper, the dynamic model of multi-arm cooperative manipulators are discussed briefly in Section 2. Then, Section 3 presents the representation issues specific to multi-arm manipulator systems mounted on a single platform and handling a common object. In Section 4, the issues related to the internal forces are discussed. Then, Section 5 deals with the development of control algorithms for fixed base, free-floating and free-flying manipulator systems. Section 6 presents the test problems and the experimental set-up for the numerical simulation of the control algorithms. The simulation results for fixed-base, free-floating and free-flying manipulator systems are presented in Section 7. Finally, in Section 8, the paper is summarised.

2. DYNAMIC MODEL OF THE MULTI-ARM MANIPULATOR SYSTEMS

2.1. Notations and kinematics

The spatial operator algebra (SOA) framework[30–33] has been used to represent the dynamics model of the multi-arm unconstrained manipulator system. The general model of a multi-arm co-ordinating space manipulator system with m-robots handling a common object, which are then mounted on a completely free base, is shown in Figure 1. Each robot consists of n rigid bodies known as links. Each adjacent link is connected by means of a joint with multiple degrees of freedom. For a space manipulator system, the base is mobile with complete motion freedom, where the attitude can rotate

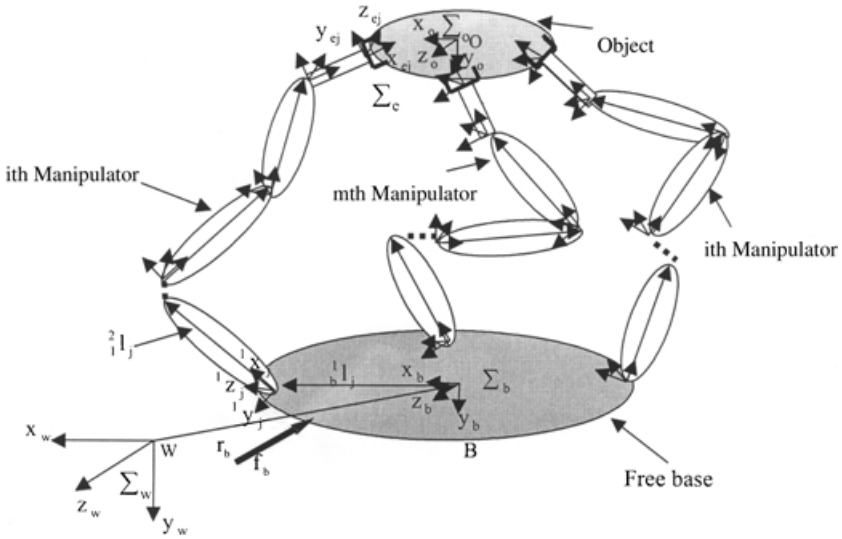

Fig. 1. A multi-arm co-ordinating space robotic system.

https://doi.org/10.1017/S0263574703005599 Published online by Cambridge University Press

about three axes as well as translate along spatial x, y and z axes, can be modelled as a six degree of freedom joint.

Without loss of generality, we have assumed that only one external spatial force $\mathbf{f}_b$ is applied to the moving platform of the system. In the absence of any external force, the momentum of the whole system can be treated as a constant. In space operation, often to conserve energy, the spacecraft thruster is closed once the robotic system acquires the required position. This type of system is called *free-floating*.[34] On the other hand, in the case of a *free-flying* manipulator system, both the spacecraft and manipulators are controlled simultaneously. Now, for the free-flying robotic systems, the spacecraft thruster force required to control its position and attitude can be equivalently modelled as an external force acting on the platform. Hence, in the case of a free-floating space robotic system, this external force can be assumed to be zero.

A space manipulator system possesses base-invariance symmetry,[35] which states that any of its constituent rigid bodies (links or spacecraft) can be chosen as a *base body* or *prime body* (PB).[36] Saha[36] has shown that the end-effector serving as a PB results in computationally efficient kinematic equations if the end-effector motion is the only concern, otherwise it is essential to choose the moving platform or the spacecraft as the PB. Thus, in this paper, the spacecraft is chosen as the PB. Further, in this paper, both manipulator joint motion variables (relative translation or rotation) and spacecraft motion variables constitute the generalized co-ordinate vector. The co-ordinate frames associated with all the variables are shown in Figure 1.

The transformation matrix for the multi-arm manipulator system can be given by[37]

$$\mathbf{X} = \mathrm{diag}(\mathbf{X}_1 \mathbf{X}_2 \ldots \mathbf{X}_m) \in \mathbb{R}^{6nm \times 6nm}$$

where $\mathbf{X}_k \in \mathbb{R}^{6n \times 6n}$ for $k \in (1, \ldots m)$ are lower triangular matrices whose elements consist of transformation matrices ${}^{i}_{i-1}\mathbf{X}_j \in \mathbb{R}^{6\times 6}$.

The end-effector spatial velocity expressed in the end-effector frame can be represented as

$$\mathbf{V}_e = \mathbf{B}\mathbf{X}_b\mathbf{V}_b + \mathbf{B}\mathbf{X}\Phi\dot{\mathbf{q}} = \mathbf{J}_b\mathbf{V}_b + \mathbf{J}_q\dot{\mathbf{q}} \tag{1}$$

where $\mathbf{J}_b \in \mathbb{R}^{6m\times 6}$ is the base Jacobian, $\mathbf{J}_b \in \mathbb{R}^{6m\times d_m}$ is the link Jacobian and $\mathbf{B} = \mathrm{diag}(\mathbf{B}_1\mathbf{B}_2 \ldots \mathbf{B}_m) \in \mathbb{R}^{6m\times 6nm}$, $\mathbf{B}_j = [\mathbf{0} \ldots \mathbf{0}\ {}^{n+1}_{n}\mathbf{X}_j] \in \mathbb{R}^{6\times 6n}$, $\mathbf{V} = [\mathbf{V}_1^T \mathbf{V}_2^T \ldots \mathbf{V}_m^T]^T \in \mathbb{R}^{6nm}$, $\mathbf{X}_b = [{}_b\mathbf{X}_1^T\ {}_b\mathbf{X}_2^T \ldots {}_b\mathbf{X}_m^T]^T \in \mathbb{R}^{6nm\times 6}$, modal matrix $\Phi = \mathrm{diag}(\Phi_1\Phi_2 \ldots \Phi_m) \in \mathbb{R}^{6nm\times d_m}$, and $\dot{\mathbf{q}} = [\dot{\mathbf{q}}_1^T\dot{\mathbf{q}}_2^T \ldots \dot{\mathbf{q}}_m^T]^T \in \mathbb{R}^{d_m}$. Hence, $\mathbf{J}_b = \mathbf{B}\mathbf{X}_b$ and $\mathbf{J}_q = \mathbf{B}\mathbf{X}\Phi$. Here, the subscripts b and q stand for base and link joints, respectively.

2.2. Base dynamics

From Figure 1, the external base force $\mathbf{f}_b \in \mathbb{R}^6$ acting on the CM of the base can be represented by

$$\mathbf{f}_b = \mathbf{M}_b\dot{\mathbf{V}}_b + \mathbf{b}_b + \mathbf{X}_b^T(\mathbf{D}\mathbf{f}_e + \mathbf{M}_q\dot{\mathbf{V}} + \mathbf{b}) \tag{2}$$

where $\mathbf{M}_b \in \mathbb{R}^{6\times 6}$ is the base inertial matrix, $\dot{\mathbf{V}}_b \in \mathbb{R}^6$ is the base acceleration, and $\mathbf{b}_b = \frac{\mathrm{d}}{\mathrm{dt}}(\mathbf{M}_b)\mathbf{V}_b \in \mathbb{R}^6$ is the base bias force.

Now, the base acceleration from Equation (2) can be expressed as

$$\dot{\mathbf{V}}_b = \mathbf{M}_b^{-1}\{\mathbf{f}_b - \mathbf{b}_b - \mathbf{X}_b^T(\mathbf{D}\mathbf{f}_c + \mathbf{M}_q\dot{\mathbf{V}} + \mathbf{b})\} \tag{3}$$

2.3. Equations of motion

Now, by using equations described above, the inverse dynamics equation is given as

$$\hat{\mathbf{T}} - \mathbf{J}^T\mathbf{f}_c = \mathbf{M}\ddot{\mathbf{q}} + \mathbf{C} \tag{4}$$

where $\mathbf{M}$ is the generalised inertia tensor, $\mathbf{J}$ is the generalised Jacobian matrix, $\mathbf{C}$ is the coriolis and centrifugal force vector, and $\hat{\mathbf{T}}$ is the vector consisting of the external base force $\mathbf{f}_b$ and joint torque vector $\mathbf{T}$.

2.4. Object dynamics

An object is assumed to be held rigidly by m manipulators. The FBD of the object is shown in Figure 2. Then, the net generalised force at the centre of mass of the object, due to all the end-effector forces acting on it, can be represented as[21,38]

$$\mathbf{f}_o = \mathbf{W}^T\mathbf{f}_e \tag{5}$$

where $\mathbf{W}^T = [{}^{n+1}_{n+2}\mathbf{X}_1^T\ {}^{n+1}_{n+2}\mathbf{X}_2^T \ldots {}^{n+1}_{n+2}\mathbf{X}_m^T] \in \mathbb{R}^{6\times 6m}$, with (n+2)th and (n+1)th joint representing object centre of mass and end-effector contact point with the object, respectively; $\mathbf{f}_o = [\eta_o^T\ f_o^T]^T \in \mathbb{R}^6$, with $f_o \in \mathbb{R}^3$ and $\eta_o \in \mathbb{R}^3$ the force and moment vectors at the object centre of mass. The positive definite matrix $\mathbf{W}$ is known as the grip matrix or grasp matrix, which is non-singular.

Now, the transformation matrix ${}^{n+1}_{n+2}\mathbf{X}_j^T = {}^{n+2}_{n+1}\mathbf{X}_j$ transforms the contact force of the jth manipulator to its equivalent at the centre of mass of the object. This can be defined as

$${}^{n+2}_{n+1}\mathbf{X}_j = \begin{bmatrix} \mathbf{E}_3 & \mathbf{0}_3 \\ \zeta_j(\mathbf{q}_j) & \mathbf{E}_3 \end{bmatrix} \tag{6}$$

where $\mathbf{E}_3$ and $\mathbf{0}_3$ are 3×3 identity and zero matrices, respectively, and

$$\zeta_j(\mathbf{q}_j) = \begin{bmatrix} 0 & {}^{n+2}_{n+1}p_{j,z} & -{}^{n+2}_{n+1}p_{j,y} \\ -{}^{n+2}_{n+1}p_{j,z} & 0 & {}^{n+2}_{n+1}p_{j,x} \\ {}^{n+2}_{n+1}p_{j,y} & -{}^{n+2}_{n+1}p_{j,x} & 0 \end{bmatrix} \tag{7}$$

where, ${}^{n+2}_{n+1}\mathbf{p}_j$ is the vector from the jth end-effector to the centre of mass (CM) of the object and is represented in the base frame.

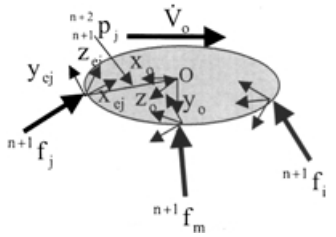

Fig. 2. Free body diagram of the object held by m manipulators.

https://doi.org/10.1017/S0263574703005599 Published online by Cambridge University Press

The force balance equation for this object from its FBD in Figure 2, can be represented as

$$\mathbf{f}_o = \mathbf{M}_o \dot{\mathbf{V}}_o + \mathbf{b}_o \tag{8}$$

where $\mathbf{M}_o \in \mathbb{R}^{6\times 6}$ is the object inertia matrix and $\mathbf{b}_o = \frac{d}{dt}(\mathbf{M}_o)$ $\mathbf{V}_o \in \mathbb{R}^6$ is the bias force on the object required to produce zero object acceleration.

Now combining Equations (5) and (8), the dynamic equation for the object can be obtained as

$$\mathbf{M}_o \dot{\mathbf{V}}_o + \mathbf{b}_o = \mathbf{W}^T \mathbf{f}_e \tag{9}$$

3. POSITION AND ORIENTATION REPRESENTATIONS

3.1. Base

The base position and orientation vector $\mathbf{x}_b \in \mathbb{R}^6$ with respect to an inertially fixed reference frame Σ_w, can be expressed as

$$\mathbf{x}_b = [\psi_b^T \quad \mathbf{r}_b^T]^T \tag{10}$$

where $\psi_b = [\alpha_b \ \ \beta_b \ \ \gamma_b]^T \in \mathbb{R}^3$ is the Euler 3-2-1 angle representation for the orientation of the base, with α_b, β_b, and γ_b being the rotations around x-, y- and z-axes, respectively. Now, the spatial base velocity $\mathbf{V}_b$ can be represented as[39]

$$\mathbf{V}_b = \mathbf{T}_B \dot{\mathbf{x}}_b \tag{11}$$

where $\mathbf{T}_B = \text{diag}(\mathbf{T}_b \ \ \mathbf{E}_3) \in \mathbb{R}^{6\times 6}$, such that the base angular velocity $\omega_b = \mathbf{T}_B \dot{\psi}_b \in \mathbb{R}^3$.

Here, the base acceleration $\dot{\mathbf{V}}_b$ can be obtained by differentiating Equation (11) so that

$$\dot{\mathbf{V}}_b = \mathbf{T}_B \ddot{\mathbf{x}}_b + \dot{\mathbf{T}}_B \dot{\mathbf{x}}_b \tag{12}$$

3.2. Object

The spatial velocity of the object can be expressed as

$$\mathbf{V}_o = \mathbf{T}_O \dot{\mathbf{x}}_o \tag{13}$$

where $\mathbf{T}_O = \text{diag}(\mathbf{T}_o \ \ \mathbf{E}_3)$, such that the angular velocity of the object $\omega_o = \mathbf{T}_o \dot{\psi}_o$, $\mathbf{x}_o = [\mathbf{r}_o^T \ \ \psi_o^T]^T$.

Now, the object acceleration can be obtained from the time derivative of Equation (13):

$$\dot{\mathbf{V}}_o = \mathbf{T}_O \ddot{\mathbf{x}}_o + \dot{\mathbf{T}}_O \dot{\mathbf{x}}_o \tag{14}$$

3.3. Object and end-effector relationship

It was emphasised in Section 2.4 that the grasp matrix $\mathbf{W}$ consists of the transformation matrices between the end-effector space (Σ_e) and the object space (Σ_o). Now, for the formulation of the $\mathbf{W}$ matrix, consider a planar rigid body (object) tightly held by two manipulators as shown in Figure 3. Here, the phase angle due to the rotation about the z-axis is γ_o. From Figure 3, let the magnitude of the length of the distance between the origin of the end-effector frame and the CM of the object be l_e for both the manipulators. Then, the vector ${}^o_e\mathbf{p}_1$ describing the position of the CM of the object with respect to the end-effector of the first manipulator can be represented as

$${}^o_e\mathbf{p}_1 = [-l_e \cos(\gamma_o) \ -l_e \sin(\gamma_o) 0]^T \tag{15}$$

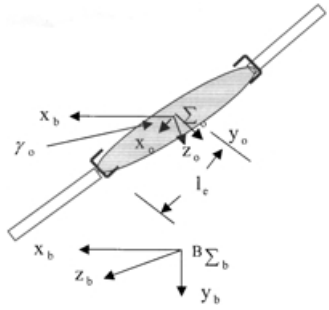

Fig. 3. A planar rigid body manipulated by two end-effectors.

Similarly, for the second manipulator it can be expressed as

$${}^o_e\mathbf{p}_2 = [l_e \cos(\gamma_o) \ l_e \sin(\gamma_o) 0]^T \tag{16}$$

Now, the $\mathbf{W}^T$ matrix can be represented as

$$\mathbf{W}^T = [{}^{n+2}_{n+1}\mathbf{X}_1 \ {}^{n+2}_{n+1}\mathbf{X}_2] =$$

$$\begin{bmatrix} 1 & 0 & 0 & 0 & 0 & 0 \\ 0 & 1 & 0 & 0 & 0 & 0 \\ 0 & 0 & 1 & 0 & 0 & 0 \\ 0 & 0 & l_e \sin(\gamma_o) & 1 & 0 & 0 \\ 0 & 0 & -l_e \cos(\gamma_o) & 0 & 1 & 0 \\ -l_e \sin(\gamma_o) & l_e \cos(\gamma_o) & 0 & 0 & 0 & 1 \end{bmatrix}$$

$$\begin{bmatrix} 1 & 0 & 0 & 0 & 0 & 0 \\ 0 & 1 & 0 & 0 & 0 & 0 \\ 0 & 0 & 1 & 0 & 0 & 0 \\ 0 & 0 & -l_e \sin(\gamma_o) & 1 & 0 & 0 \\ 0 & 0 & l_e \cos(\gamma_o) & 0 & 1 & 0 \\ l_e \sin(\gamma_o) & l_e \cos(\gamma_o) & 0 & 0 & 0 & 1 \end{bmatrix} \tag{17}$$

The end-effector velocity vector presented in Equation (1) is described in the end-effector frame. But, this can be represented in the base frame as

$$\begin{aligned} \mathbf{V}_e &= \mathbf{R}_b \mathbf{B} \mathbf{X}_b \mathbf{V}_b + \mathbf{R}_b \mathbf{B} \mathbf{X} \Phi \dot{\mathbf{q}} \\ &= \bar{\mathbf{J}}_b \mathbf{V}_b + \bar{\mathbf{J}}_q \dot{\mathbf{q}} \end{aligned} \tag{18}$$

where $\mathbf{R}_b = \text{diag}({}^b_{n+1}\mathbf{R}_1 \ {}^b_{n+1}\mathbf{R}_1 \ldots {}^b_{n+1}\mathbf{R}_m \ {}^b_{n+1}\mathbf{R}_m) \in \mathbb{R}^{6m\times 6m}$ with ${}^b_{n+1}\mathbf{R}_j \in \mathbb{R}^3$ as the rotation matrix of the end-effector frame of the jth manipulator with respect to the base frame.

4. INTERNAL FORCE REPRESENTATION

The total end-effector force $\mathbf{f}_e$ is calculated from Equation (4), and can now be decomposed into a motion-inducing part or *motive force* $\mathbf{f}_e^m$, and an internal force component $\mathbf{f}_e^i$. This can be represented as:

$$\mathbf{f}_e = \mathbf{f}_e^m + \mathbf{f}_e^i \tag{19}$$

Now, the force $\mathbf{f}_o$ acting on the CM of the object represented in the frame Σ_o can be expressed from Equation (5) as

$$\mathbf{f}_o = \mathbf{W}^T(\mathbf{f}_e^m + \mathbf{f}_e^i) = \mathbf{W}^T \mathbf{f}_e^m \tag{20}$$

where $\mathbf{W}^T \mathbf{f}_e^i = \mathbf{0}$, due to the fact that all the internal forces now will cancel each other and their net effect in the common frame Σ_o is zero.

https://doi.org/10.1017/S0263574703005599 Published online by Cambridge University Press

Then, from Equation (20) the motion-inducing force $\mathbf{f}_e^m$ can be represented as

$$\begin{aligned}\mathbf{f}_e^m &= (\mathbf{W}^T)^{\#}\mathbf{f}_o \\ &= (\mathbf{W}^T)^{\#}\mathbf{W}^T\mathbf{f}_e\end{aligned} \tag{21}$$

where $(\mathbf{W}^T)^{\#}$ is the pseudo-inverse of the matrix $\mathbf{W}^T$.

Now, the internal force $\mathbf{f}_e^i$ can be represented as

$$\mathbf{f}_e^i = (\mathbf{E}_{6m} - (\mathbf{W}^T)^{\#}\mathbf{W}^T)\mathbf{f}_e \tag{22}$$

where $\mathbf{E}_{6m} \in \mathbb{R}^{6m \times 6m}$ is an identity matrix.

Now, From Equation (22), it can be observed that the internal forces are the projections of the end-effector forces into the null-space of $\mathbf{W}^T$, i.e. $\mathbf{W}^T\mathbf{f}_e^i = \mathbf{0}$.

Walker *et al.*[40] showed that the weighting matrix $\mathbf{W}^T$ should be chosen judiciously so that the motion-inducing and internal force components are completely separate from each other. A unit-weighting matrix that is normally used for pseudo-inverse calculations of a given matrix does not yield a so-called *no-squeeze solution*.[40] Walker *et al.*[40] suggested a weighting matrix such that the pseudo-inversion of $\mathbf{W}^T$ can be expressed as

$$(\mathbf{W}^T)^{\#} = \frac{1}{m}\begin{bmatrix} \mathbf{E}_3 & \mathbf{0} \\ -\zeta_1 & \mathbf{E}_3 \\ \cdot & \cdot \\ \cdot & \cdot \\ \mathbf{E}_3 & \mathbf{0} \\ -\zeta_m & \mathbf{E}_3 \end{bmatrix} = \frac{1}{m}\begin{bmatrix} \mathbf{W}_1^{-T} \\ \cdot \\ \cdot \\ \cdot \\ \mathbf{W}_m^{-T} \end{bmatrix} \tag{23}$$

The pseudo-inverse solution in Equation (23) is known as a no-squeeze solution and thus results in zero internal forces and moments. Then, the use of Equation (23) in Equations (21) and (22) results in the pure motion-inducing and pure internal components of the external forces acting on the object by the end-effectors.

5. DEVELOPMENT OF CONTROL ALGORITHMS

In co-operating manipulator systems, the end-effectors are subject to external forces due to the interaction with the environment (object). Thus, it is necessary to include the effects of the end-effector forces in the inverse dynamics control algorithms.

The block diagram representation of the inverse dynamics control method for co-operating manipulators is shown in Figure 4. The controller accepts the values of all the desired and actual object and/or base position and orientation related information along with the end-effector forces to calculate the resolved acceleration vector **a**. Then, the block representing the inverse dynamics control law provides the necessary torques to be applied to the active joints and/or base.

5.1. Multi-arm fixed-base manipulator systems

The inverse dynamics equation of a multi-arm, fixed-base manipulator system for non-null contact force is given by

$$\mathbf{T} - \mathbf{J}^T\mathbf{f}_e = \mathbf{M}\ddot{\mathbf{q}} + \mathbf{C} \tag{24}$$

Now, the inverse dynamics control law for this system can be expressed as

$$\ddot{\mathbf{q}} = \mathbf{u} - \mathbf{M}^{-1}\mathbf{J}^T\mathbf{f}_e \tag{25}$$

where **u** is the resolved acceleration in terms of the joint variable. In Equation (25), the factor $\mathbf{M}^{-1}\mathbf{J}^T\mathbf{f}_e$ serves as the nonlinear coupling term due to the presence of the end-effector force vector $\mathbf{f}_e$. Then, the linearity and the decoupling of the inverse dynamics controllers can be maintained by the following selection of the control torque:

$$\mathbf{T} = \mathbf{M}\mathbf{u} + \mathbf{C} + \mathbf{J}^T\mathbf{f}_e \tag{26}$$

where the control input **u** can be expressed as

$$\mathbf{u} = \bar{\mathbf{J}}_q^{\#}(\mathbf{a} - \dot{\mathbf{J}}_q\dot{\mathbf{q}}) \tag{27}$$

and the resolved acceleration **a** can be chosen such that the end-effectors will track the desired trajectories perfectly.

Now, the use of Equation (26) exactly compensates the contact force $\mathbf{f}_e$, thereby making the end-effector infinitely stiff with respect to the object. However, the co-operating control of the multiple manipulators holding a common object requires internal forces to keep hold of the object. Hence, in this work, the internal forces are not compensated. Thus, the control torques are chosen as

$$\begin{aligned}\mathbf{T} &= \mathbf{M}\mathbf{u} + \mathbf{C} + \mathbf{J}^T(\mathbf{f}_e - \mathbf{f}_e^i) \\ &= \mathbf{M}\mathbf{u} + \mathbf{C} + \mathbf{J}^T\mathbf{f}_e^m\end{aligned} \tag{28}$$

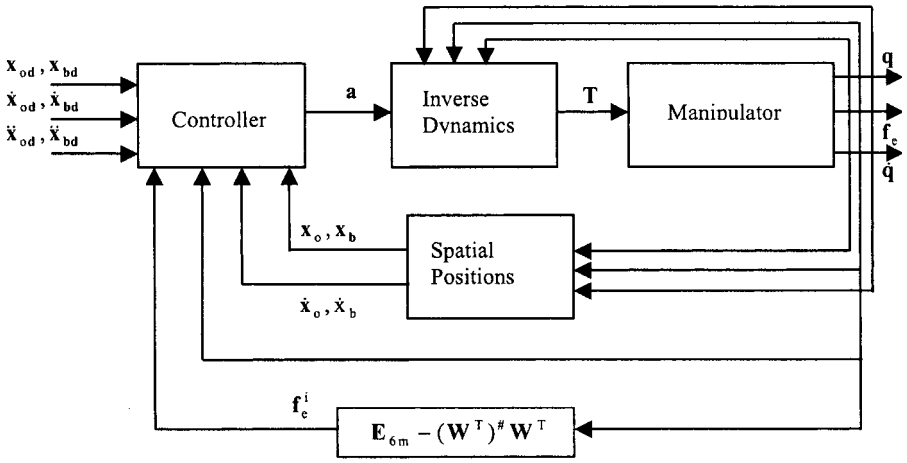

Fig. 4. Block diagram of inverse dynamics control scheme for co-operating manipulator systems.

https://doi.org/10.1017/S0263574703005599 Published online by Cambridge University Press

where $\mathbf{u}$ and the resolved acceleration $\mathbf{a}$ are chosen in terms of the joint variables.

For the convenience of the control of the position and orientation of the object centre of mass (CM), it is required to represent Equations (24) to (27) directly in terms of the object variables. This representation is shown in the following Lemma 1.

Lemma 1: The equations of motion for a co-operating, fixed-base, rigid-link, multi-arm manipulator system can be described as

$$\mathbf{T}=\mathbf{M}_{op}\ddot{\mathbf{x}}_o+\mathbf{C}_{op}+\mathbf{J}^T\mathbf{f}_e \tag{29}$$

where

$$\mathbf{M}_{op}=\mathbf{M}\bar{\mathbf{J}}_p^{\#}\mathbf{W}\mathbf{T}_O, \tag{30}$$

and

$$\mathbf{C}_{op}=\mathbf{M}\bar{\mathbf{J}}_q^{\#}\left\{\frac{d}{dt}(\mathbf{W}\mathbf{T}_O)-\dot{\bar{\mathbf{J}}}_q\bar{\mathbf{J}}_q^{\#}\mathbf{W}\mathbf{T}_O\right\}\dot{\mathbf{x}}_o+\mathbf{C} \tag{31}$$

Proof: Now, the Equations (13) and (18) yield

$$\mathbf{V}_e=\bar{\mathbf{J}}_q\dot{\mathbf{q}}=\mathbf{W}\mathbf{T}_O\dot{\mathbf{x}}_o \tag{32}$$

The time derivative of Equation (32) gives

$$\ddot{\mathbf{q}}=\bar{\mathbf{J}}_q^{\#}\left\{\mathbf{W}\mathbf{T}_O\ddot{\mathbf{x}}_o+\frac{d}{dt}(\mathbf{W}\mathbf{T}_O)\dot{\mathbf{x}}_o-\dot{\bar{\mathbf{J}}}_q\bar{\mathbf{J}}_q^{\#}\mathbf{W}\mathbf{T}_O\dot{\mathbf{x}}_o\right\} \tag{33}$$

Then, substituting Equation (33) into Equation (24), gives

$$\mathbf{T}=\mathbf{M}_{op}\ddot{\mathbf{x}}_o+\mathbf{C}_{op}+\mathbf{J}^T\mathbf{f}_e$$

where the terms $\mathbf{M}_{op}$ and $\mathbf{C}_{op}$ are defined by Equations (30) and (31).

Now, the proposed control law to control the object motion can be given by

$$\mathbf{u}=\bar{\mathbf{J}}_q^{\#}\mathbf{W}\mathbf{T}_O\{\ddot{\mathbf{x}}_{od}+\mathbf{K}_d(\dot{\mathbf{x}}_{od}-\dot{\mathbf{x}}_o)+\mathbf{K}_p(\mathbf{x}_{od}-\mathbf{x}_o)\}$$

$$+\bar{\mathbf{J}}_q^{\#}\left\{\frac{d}{dt}(\mathbf{W}\mathbf{T}_O)-\dot{\bar{\mathbf{J}}}_q\bar{\mathbf{J}}_q^{\#}\mathbf{W}\mathbf{T}_O\right\}\dot{\mathbf{x}}_o \tag{34}$$

where $\mathbf{K}_p$ and $\mathbf{K}_d$ are proportional and derivative feedback gain matrices, respectively.

4.2. Multi-arm free-floating manipulator systems

The equations of motion of a co-ordinating, rigid-link, multi-arm, free-floating space manipulator system can be represented from Equations (1) and (4) as

$$\mathbf{T}=\mathbf{M}\ddot{\mathbf{q}}+\mathbf{C}+\mathbf{J}^T\mathbf{f}_e \tag{35}$$

$$\dot{\mathbf{V}}_e=\bar{\mathbf{J}}_b\dot{\mathbf{V}}_b+\dot{\bar{\mathbf{J}}}_b\mathbf{V}_b+\bar{\mathbf{J}}_q\ddot{\mathbf{q}}+\dot{\bar{\mathbf{J}}}_q\dot{\mathbf{q}} \tag{36}$$

These equations are obtained by substituting $\mathbf{f}_b=\mathbf{0}$. Here, the base velocity is represented in the base frame. in Equation (11), the base velocity $\mathbf{V}_b$ in terms of $\dot{\mathbf{x}}_b$ is represented in the frame Σ_w. Thus, the base velocity in Equation (36) in Σ_w frame can be represented as

$$\mathbf{V}_b=\mathbf{R}_w^{-1}\mathbf{T}_B\dot{\mathbf{x}}_b \tag{37}$$

where $\mathbf{R}_w=\mathrm{diag}({}^w_b\mathbf{R}\ {}^w_b\mathbf{R})\in\mathbb{R}^{6\times6}$ with ${}^w_b\mathbf{R}\in\mathbb{R}^{3\times3}$ denoting the rotation of the base frame Σ_b with respect to Σ_w.

Then, the base acceleration can be obtained by differentiating Equation (37) with respect to time:

$$\dot{\mathbf{V}}_b=\frac{d}{dt}(\mathbf{R}_w^{-1}\mathbf{T}_B\dot{\mathbf{x}}_b)=\mathbf{R}_w^{-1}\mathbf{T}_B\ddot{\mathbf{x}}_b+(\dot{\mathbf{R}}_w^{-1}\mathbf{T}_B+\mathbf{R}_w^{-1}\dot{\mathbf{T}}_B)\dot{\mathbf{x}}_b \tag{38}$$

Hence, the end-effector velocity $\mathbf{V}_e$ can be represented from Equation (l) by

$$\mathbf{V}_e=\bar{\mathbf{J}}_b\mathbf{R}_w^{-1}\mathbf{T}_B\dot{\mathbf{x}}_b+\dot{\bar{\mathbf{J}}}_q\dot{\mathbf{q}} \tag{39}$$

Using the principle of virtual work from classical mechanics that establishes the duality between forces and velocities, the end-effector velocity can be expressed as

$$\mathbf{V}_e=\mathbf{W}\mathbf{V}_0 \tag{40}$$

where $\mathbf{V}_0\in\mathbb{R}^6$ is the velocity of the CM of the object. Then, the end-effector acceleration $\dot{\mathbf{V}}_e$ in Equation (36) can be rewritten as

$$\dot{\mathbf{V}}_e=\bar{\mathbf{J}}_b\mathbf{R}_w^{-1}\mathbf{T}_B\ddot{\mathbf{x}}_b+\bar{\mathbf{J}}_b(\dot{\mathbf{R}}_w^{-1}\mathbf{T}_B+\mathbf{R}_w^{-1}\dot{\mathbf{T}}_B)\dot{\mathbf{x}}_b$$
$$+\dot{\bar{\mathbf{J}}}_b\mathbf{R}_w^{-1}\mathbf{T}_B\dot{\mathbf{x}}_b+\bar{\mathbf{J}}_q\ddot{\mathbf{q}}+\dot{\bar{\mathbf{J}}}_q\dot{\mathbf{q}} \tag{41}$$

Moreover, to control the end-effector motion, Equation (35) must be expressed in terms of the end-effector motion variables. This can be described by the following results.

Lemma 2: The equations of motion suitable for the end-effector motion control of the co-operating, rigid-link, multi-arm, free-floating space manipulator system can be represented as

$$\mathbf{T}=\mathbf{M}_{op}\ddot{\mathbf{x}}_o+\mathbf{C}_{op}+\mathbf{J}^T\mathbf{f}_e \tag{42}$$

where

$$\mathbf{M}_{op}=\mathbf{M}(\bar{\mathbf{J}}_q-\bar{\mathbf{J}}_b\mathbf{M}_b^{-1}\mathbf{X}_b^T\mathbf{M}_x\mathbf{X}\Phi)_{-1}\mathbf{W}\mathbf{T}_O \tag{43}$$

$$\mathbf{M}_x=\mathbf{M}_q(\mathbf{E}+\mathbf{X}_b\mathbf{M}_b^{-1}\mathbf{X}_b^T\mathbf{M}_q)^{-1} \tag{44}$$

$$\mathbf{C}_{op}=\mathbf{M}_{op}(\mathbf{W}\mathbf{T}_O)^{-1}[\{\dot{\bar{\mathbf{J}}}_q\bar{\mathbf{J}}_q^{\#}\bar{\mathbf{J}}_b-\dot{\bar{\mathbf{J}}}_b+\bar{\mathbf{J}}_b\mathbf{M}_b^{-1}\mathbf{X}_b^T\mathbf{M}_x$$
$$(\dot{\mathbf{X}}_b-\dot{\mathbf{X}}\Phi\bar{\mathbf{J}}_q^{\#}\bar{\mathbf{J}}_b\}\times\mathbf{R}_w^{-1}\mathbf{T}_B\dot{\mathbf{x}}_b+(\bar{\mathbf{J}}_b\mathbf{M}_b^{-1}\mathbf{X}_b^T\mathbf{M}_x\dot{\mathbf{X}}\Phi$$
$$-\dot{\bar{\mathbf{J}}}_q)\bar{\mathbf{J}}_q^{\#}\mathbf{W}\mathbf{T}_O\dot{\mathbf{x}}_o+\bar{\mathbf{J}}_b\mathbf{J}'(\mathbf{b}_b+\mathbf{X}_b^T\mathbf{b})]+\mathbf{C} \tag{45}$$

$$\mathbf{J}'=\mathbf{M}_b^{-1}(\mathbf{E}_6-\mathbf{X}_b^T\mathbf{M}_x\mathbf{X}_b\mathbf{M}_b^{-1}) \tag{46}$$

Proof: The proof of this lemma can be achieved as follows.

Now, Equations (1), (13) and (40) yields

$$\mathbf{V}_e=\bar{\mathbf{J}}_b\mathbf{V}_b+\bar{\mathbf{J}}_q\dot{\mathbf{q}}=\mathbf{W}\mathbf{T}_O\dot{\mathbf{x}}_o \tag{47}$$

The time derivative of Equation (47) gives

$$\bar{\mathbf{J}}_b\dot{\mathbf{V}}_b+\dot{\bar{\mathbf{J}}}_b\mathbf{V}_b+\dot{\bar{\mathbf{J}}}_q\dot{\mathbf{q}}+\bar{\mathbf{J}}_q\ddot{\mathbf{q}}=\mathbf{W}\mathbf{T}_O\ddot{\mathbf{x}}_o+\frac{d}{dt}(\mathbf{W}\mathbf{T}_O)\dot{\mathbf{x}}_o \tag{48}$$

Then, using Equations (3), (12), (35), (36) and (48), the following expressions can be obtained

$$\mathbf{T}=\mathbf{M}\ddot{\mathbf{q}}+\mathbf{C}+\mathbf{J}^T\mathbf{f}_e$$

where $\mathbf{M}_{op}$ and $\mathbf{C}_{op}$ are defined as in Equations (43) to (46).

https://doi.org/10.1017/S0263574703005599 Published online by Cambridge University Press

Now, to control the object motion, the control law can be given as

$$\begin{aligned}\mathbf{u} &= (\bar{\mathbf{J}}_q - \bar{\mathbf{J}}_b\mathbf{M}_b^{-1}\mathbf{X}_b^T\mathbf{M}_x\mathbf{X}\Phi)^{-1}\mathbf{W}\mathbf{T}_O \\ &\times [\{\ddot{\mathbf{x}}_{od} + \mathbf{K}_d(\dot{\mathbf{x}}_{od} - \dot{\mathbf{x}}_o) + \mathbf{K}_p(\mathbf{x}_{od} - \mathbf{x}_o)\} + (\mathbf{W}\mathbf{T}_O)^{-1} \\ &\times [\{\dot{\bar{\mathbf{J}}}_q\bar{\mathbf{J}}_q^{\#}\bar{\mathbf{J}}_b - \bar{\mathbf{J}} + \bar{\mathbf{J}}_b\mathbf{M}_b^{-1}\mathbf{X}_b^T\mathbf{M}_x(\dot{\mathbf{X}}_b - \dot{\mathbf{X}}\Phi\bar{\mathbf{J}}_q^{\#}\bar{\mathbf{J}}_b\}\mathbf{R}_w^{-1}\mathbf{T}_B\dot{\mathbf{x}}_b \\ &+ (\bar{\mathbf{J}}_b\mathbf{M}_b^{-1}\mathbf{X}_b^T\mathbf{M}_x\dot{\mathbf{X}}\Phi - \dot{\bar{\mathbf{J}}}_q\dot{\bar{\mathbf{J}}})\bar{\mathbf{J}}\,\mathbf{W}\mathbf{T}_O\dot{\mathbf{x}}_o + \bar{\mathbf{J}}_b\mathbf{J}'(\mathbf{b}_b + \mathbf{X}_b^T\mathbf{b})]\end{aligned} \tag{49}$$

4.3. Multi-arm free-flying manipulator systems

The equations of motion of a co-operating, rigid-link, multi-arm, free-flying space manipulator system can be represented from Equation (4) as

$$\hat{\mathbf{T}} = \mathbf{M}\ddot{\mathbf{q}} + \mathbf{C} + \mathbf{J}^T\mathbf{f}_e \tag{50}$$

and the expression for $\dot{\mathbf{V}}_e$ is as given in Equation (36). Then, Equation (50) can be expressed in the following form:

$$\mathbf{L}\mathbf{T}_f = \mathbf{M}\ddot{\mathbf{q}} + \mathbf{C} + \mathbf{J}^T\mathbf{f}_e \tag{51}$$

where $\mathbf{T}_f = [\mathbf{T}^T\ \mathbf{f}_b^T]^T$, $\mathbf{L} = [\mathbf{E}_6\ \mathbf{C}']$ and $\mathbf{C}' = -\Phi^T\mathbf{X}^T(\mathbf{M}_q^{-1} + \mathbf{X}_b\mathbf{M}_b^{-1}\mathbf{X}_b^T)^{-1}\mathbf{X}_b\mathbf{M}_b^{-1}$.

The following results describe a suitable form of the equation of motion as given in Equation (51) in terms of the object and base (spacecraft) control variables.

Lemma 3: The equations of motion for a co-operating, rigid-link, multi-arm, free-flying space manipulator system can be described as

$$\mathbf{L}\mathbf{T}_f = \mathbf{M}_{op}\ddot{\mathbf{x}}_{ob} + \mathbf{C}_{op} + \mathbf{J}^T\mathbf{f}_e \tag{52}$$

where

$$\mathbf{M}_{op} = \mathbf{M}\bar{\mathbf{J}}_q^{\#}\mathbf{T}_{OB}, \tag{53}$$

$$\mathbf{C}_{op} = \mathbf{M}\bar{\mathbf{J}}_q^{\#}(\dot{\mathbf{T}}_{OB} - \dot{\bar{\mathbf{J}}}_q\bar{\mathbf{J}}_q^{\#}\mathbf{T}_{OB})\dot{\mathbf{x}}_{ob} + \mathbf{C}, \tag{54}$$

$$\mathbf{T}_{OB} = [\mathbf{W}\mathbf{T}_O \quad -\bar{\mathbf{J}}_b\mathbf{R}_w^{-1}\mathbf{T}_B], \tag{55}$$

and the symbols $\mathbf{L}$ and $\mathbf{T}_f$ are described after Equation (51).

Proof: Here, Equation (47) can produce

$$\mathbf{V}_e = \bar{\mathbf{J}}_b\mathbf{R}_w^{-1}\mathbf{T}_B\dot{\mathbf{x}}_b + \bar{\mathbf{J}}_q\dot{\mathbf{q}} = \mathbf{W}\mathbf{T}_O\dot{\mathbf{x}}_o \tag{56}$$

Now, Equation (56) can be represented as

$$\mathbf{T}_{OB}\dot{\mathbf{x}}_{ob} = \bar{\mathbf{J}}_q\dot{\mathbf{q}} \tag{57}$$

where $\mathbf{T}_{OB} = [\mathbf{W}\mathbf{T}_O - \bar{\mathbf{J}}_b\mathbf{R}_w^{-1}\mathbf{T}_B]$, and $\dot{\mathbf{x}}_{ob} = [\dot{\mathbf{x}}_o^T\ \dot{\mathbf{x}}_b^T]^T$

The time derivative of Equation (57) gives rise to

$$\bar{\mathbf{J}}_q\ddot{\mathbf{q}} = \mathbf{T}_{OB}\ddot{\mathbf{x}}_{ob} + \dot{\mathbf{T}}_{OB}\dot{\mathbf{x}}_{ob} - \dot{\bar{\mathbf{J}}}_q\dot{\mathbf{q}} \tag{58}$$

where $\ddot{\mathbf{x}}_{ob} = [\ddot{\mathbf{x}}_o^T\ \ddot{\mathbf{x}}_b^T]^T$.

Now, use of Equations (57) and (58) yields

$$\ddot{\mathbf{q}} = \bar{\mathbf{J}}_q^{\#}[\mathbf{T}_{OB}\ddot{\mathbf{x}}_{ob} + (\dot{\mathbf{T}}_{OB} - \dot{\bar{\mathbf{J}}}_q\bar{\mathbf{J}}_q^{\#}\mathbf{T}_{OB})\dot{\mathbf{x}}_{ob}] \tag{59}$$

Then, substituting Equation (59) into Equation (56), gives

$$\mathbf{L}\mathbf{T}_f = \mathbf{M}_{op}\ddot{\mathbf{x}}_{ob} + \mathbf{C}_{op} + \mathbf{J}^T\mathbf{f}_e$$

where the terms $\mathbf{L}$, $\mathbf{M}_{op}$ and $\mathbf{C}_{op}$ are defined by Equations (53) to (55).

Now, the proposed control law to control simultaneously the object and spacecraft is given by

$$\begin{aligned}\mathbf{u} &= \bar{\mathbf{J}}_q^{\#}\mathbf{T}_{OB}\{\ddot{\mathbf{x}}_{ob,d} + \mathbf{K}_d(\dot{\mathbf{x}}_{ob,d} - \dot{\mathbf{x}}_{ob}) + \mathbf{K}_p(\mathbf{x}_{ob,d} - \mathbf{x}_{ob})\} \\ &+ \bar{\mathbf{J}}_q^{\#}(\dot{\mathbf{T}}_{OB} - \dot{\bar{\mathbf{J}}}_q\bar{\mathbf{J}}_q^{\#}\mathbf{T}_{OB})\dot{\mathbf{x}}_{ob}\end{aligned} \tag{60}$$

6. SIMULATION STUDIES

6.1. Simulation environment

A two-arm manipulator system with three-links per manipulator holding an object has been shown in Figure 5. All the joints are assumed to be one-degree-of freedom rotational joints with rigid links.

Two manipulators are mounted on a free-base with a base frame Σ_b defined at the centre of mass (CM) 'B' of the free base. All the links are assumed to be of equal length ${}^{k+1}_{k}l_j = 1.0$ m. $\forall j \in \{1, 2\}$ and $\forall k \in \{1, \ldots, 3\}$. The mass and inertia of each link are ${}^{k}m_j = 1$ Kg and ${}^{k}I_j = 0.33\ \text{Kg} - \text{m}^2$, $\forall j \in \{1, 2\}$ and $\forall k \in \{1, \ldots, 3\}$, respectively. It is assumed that both the manipulators are mounted on the base such that their distances from the CM of the base 'B' are equal. Here,

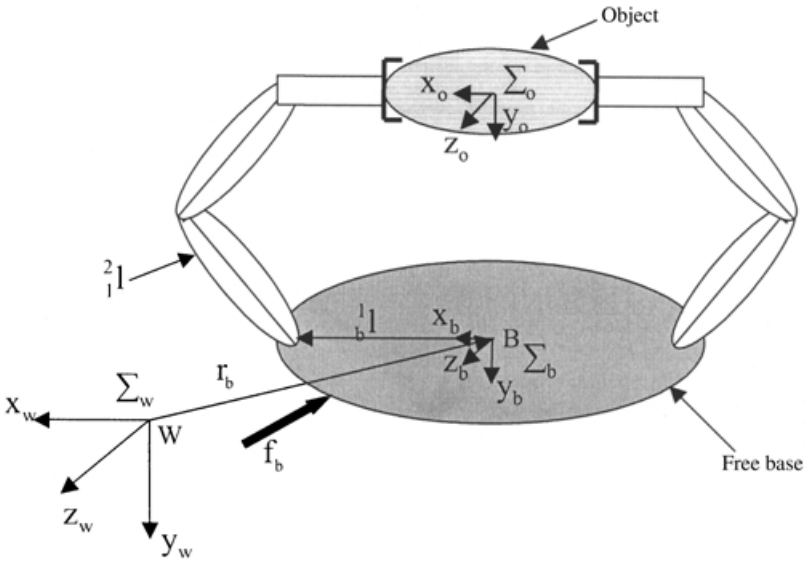

Fig. 5. Two-arm three-link co-operating manipulator system.

https://doi.org/10.1017/S0263574703005599 Published online by Cambridge University Press

this distance ${}^{1}_{b}l_j = 1.5$ m, $\forall j \in \{1, 2\}$. The mass of the base $m_b = 200$ Kg, and its inertia $I_b = 40$ Kg $-$ m^2. The mass of the object $m_o = 2$ Kg, and inertia $I_o = 0.5$ Kg $-$ m^2. Initially, the object centre-of-mass was at (0.0, –1.7320508, 0.0) metres. Corresponding to the object position, the joint angles of manipulator 1 and 2 were (–1.0471976, –1.0471976, –1.0471976) radians and (–2.0943951, 1.0471976, 1.0471976) radians, respectively. The initial object orientation about the z-axis of the base frame Σ_b was zero radians. Also, the orientations of the base frame Σ_b with respect to the world reference frame Σ_w of all the axes were zero radians. For a fixed-base manipulator system, Σ_b and Σ_w were chosen to be coincident with each other. The sampling time for all the simulations described in this research were fixed at 0.001 sec. The diagonal elements of the controller gain matrices $\mathbf{K}_p$ and $\mathbf{K}_d$ were set to 16 and 10, respectively, for all the simulation work.

6.2. *Design of test problems*

Here, two clearly distinct types of time-varying trajectories have been considered for testing the efficacy of the developed inverse dynamics controllers. The first example is a common circle problem, where both the end-effectors were assigned the task of tracking circles in space while tracking a time-varying desired orientation trajectory. The second example considered here is a modified form of trajectories defined in Egeland-Sagli.[41] Here, the modification includes a time-varying orientation trajectory in addition to the time-varying end-effector position vectors. This modified test case is called here the *augmented Egeland-Sagli* test case.

Test Problem 1: ***Circle Tracking Problem***

$$\gamma = r_1 \sin(\xi t)$$
$$p_x = d + r\cos(\xi t)$$
$$p_y = -h + r\sin(\xi t)$$

where r is the radius of the circle with centre at the co-ordinate point (d, h), r_1 is the amplitude of the orientation variation, $\xi = k\pi$, with k as a constant, γ is the end-effector orientation about the z-axis, and p_x and p_y are the x- and y-positions of the end-effector. Here, the parameters of the circle were taken as $r = 0.2$ m, $r_1 = 0.1$ m, $(d, h) = (0.0, -1.5)$ and $k = 1$.

Test Problem 2: ***Augmented Egeland-Sagli Problem***

This test case consists of position trajectories with a simple ramp, and a combination of ramp and sinusoidal components:

$$\gamma = -\pi - r\sin(\xi t)$$
$$p_x = k_1 + k_2 t$$
$$p_y = \begin{cases} h_1 + k_3 \sin(\xi t); & 0 < t \le 2s \\ h_1 + k_3 \sin(\xi t); & 2s < t \le 4s \\ h_2 + k_3 \sin(\xi t); & 4s < t \le 6s \end{cases}$$

where h_i's and k_i's are constants, and other parameters bear the same meaning as in the circle problem. In this case, the parameter values taken for the simulation study are: $r = 0.2$ m, $k = 2$, $k_1 = 0.5$, $h_1 = -1.7320508$, $k_2 = 0.1$, $k_3 = 0.05$, $h_2 = -1.5320508$.

7. RESULTS AND DISCUSSION

7.1. *Fixed-base two-arm co-operating manipulator system*

The performance of a two-arm co-operating manipulator system rigidly holding an object that tracks a circular contour in space is shown in Figures 6 to 9. Figure 6 shows the position and orientation tracking performance of the object. These results show that the object tracks the desired trajectories perfectly. The circular contour tracking in the x-y co-ordinate plane is shown in Figure 7. The actual trajectory represented by the dashed lines tracks the desired circular contour represented by the solid line in spite of starting at a completely faraway location. The input torques are shown in Figures 8(a) and (b). It can be observed from these figures that the second manipulator requires larger torques than the first manipulator. Figures 9(a) and (b) show the internal forces created during the tracking process.

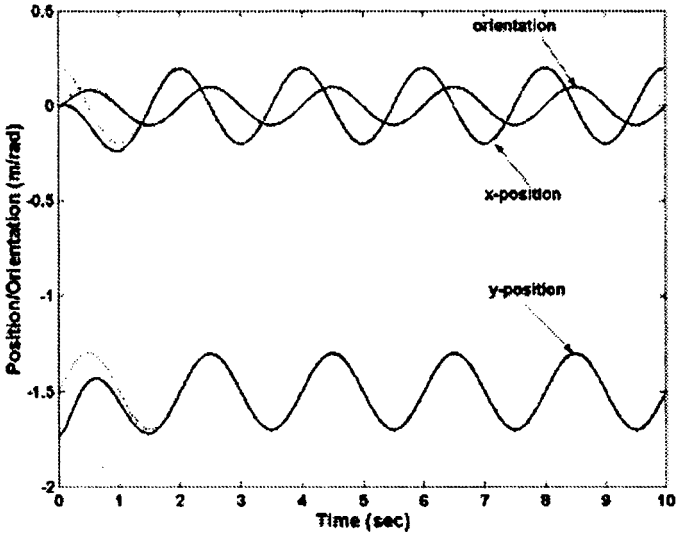

Fig. 6. Position and orientation tracking (Circle Problem). The dashed lines indicate desired and the solid lines indicate actual.

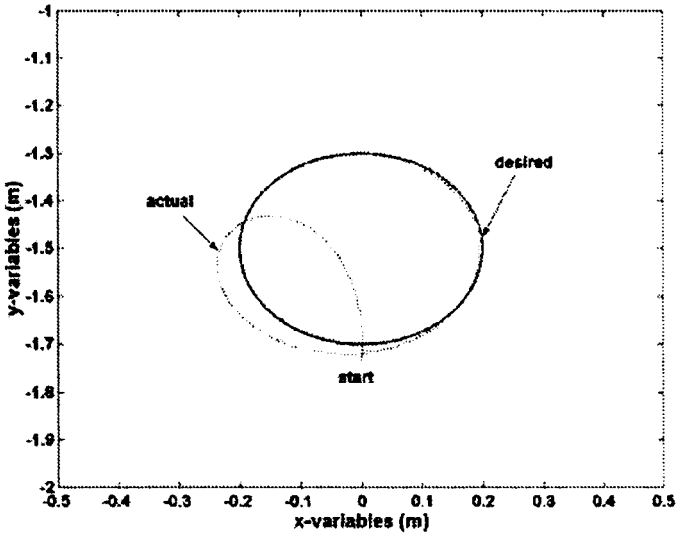

Fig. 7. Motion of the payload in Cartesian space for the fixed-base configuration.

https://doi.org/10.1017/S0263574703005599 Published online by Cambridge University Press

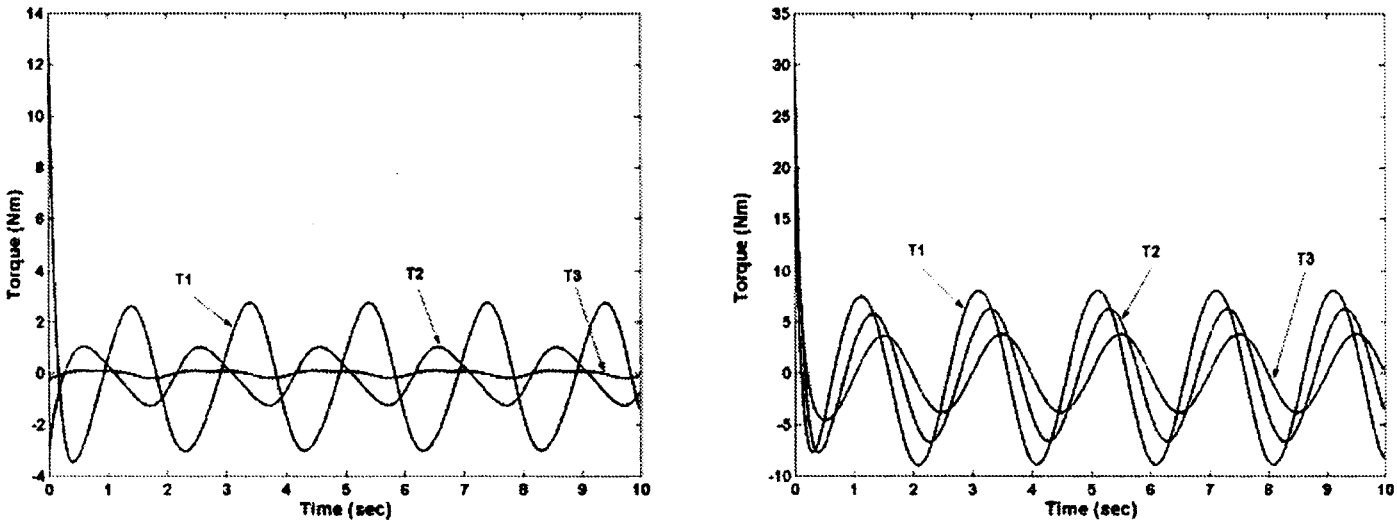

(a) Manipulator 1 (b) Manipulator 2

Fig. 8. Torque profiles for the fixed-base configuration for the circle problem.

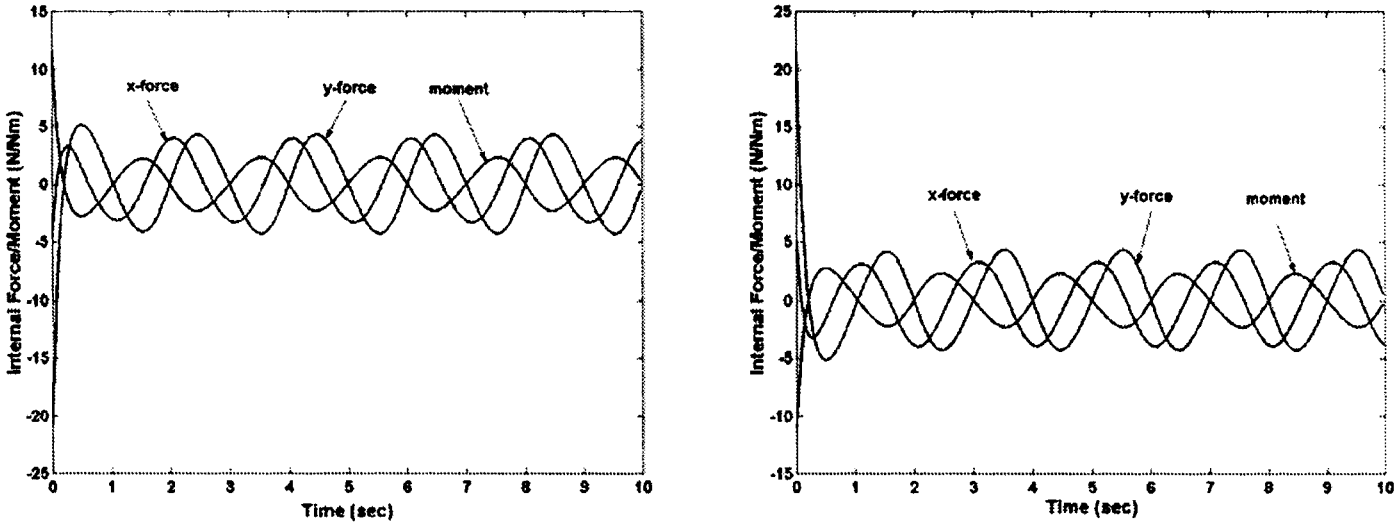

(a) At End-effector 1 (b) At End-effector 2

Fig. 9. Internal forces at the end-effector frames for a fixed-base configuration (Circle Problem).

These figures clearly show that the internal forces cancel each other at every instant of time.

Now, the tracking performances of the object on the augmented Egeland-Sagli trajectories are shown in Figures 10 to 12. Figure 10(a) illustrates the position and orientation tracking performance of the object. A clear picture of the y-position tracking is shown in Figure 10(b). These figures show the good tracking performance of the controller. The torque profiles are shown in Figures 11(a) and (b). It can be observed from the torque profiles that relatively large initial torques are needed, which only vary within a small range after about 0.2 sec. Here, the torque requirements after 0.2 sec for both the manipulators remains almost the same. The internal forces used during the tracking control operation are shown in Figures 12(a) and (b) for the first and second end-effectors, respectively. It is clear from these figures that the internal forces cancel each other at every instant of time.

7.2. Free-floating two-arm co-operating manipulator system

Interestingly enough, all the performance characteristics for the free-floating system exactly matched those for the fixed-base manipulator system on both the circular and the augmented Egeland-Sagli problem. Hence, those figures are not repeated here. Essentially, this shows that, in free-floating, co-operating space manipulator systems, the tracking control does not need any extra energy to perform exactly the same job compared to the fixed-base co-operating manipulator systems. The forces of interaction between the manipulators and the base are shown in Figure 13. For the augmented Egeland-Sagli problem, the base interaction forces at the base are shown in Figure 14. It is evident from Figures 13 and 14 that the magnitude of the base interaction forces in the case of tracking augmented Egeland-Sagli trajectories is more than that for the circle-tracking problem. ‘

https://doi.org/10.1017/S0263574703005599 Published online by Cambridge University Press

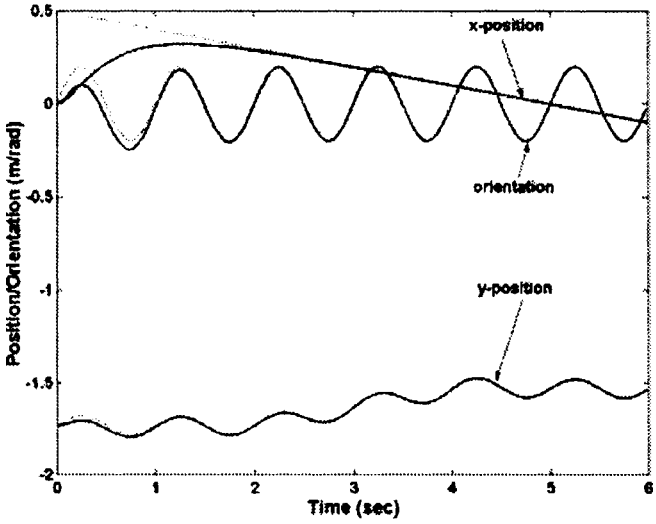

(a) Position and Orientation Tracking

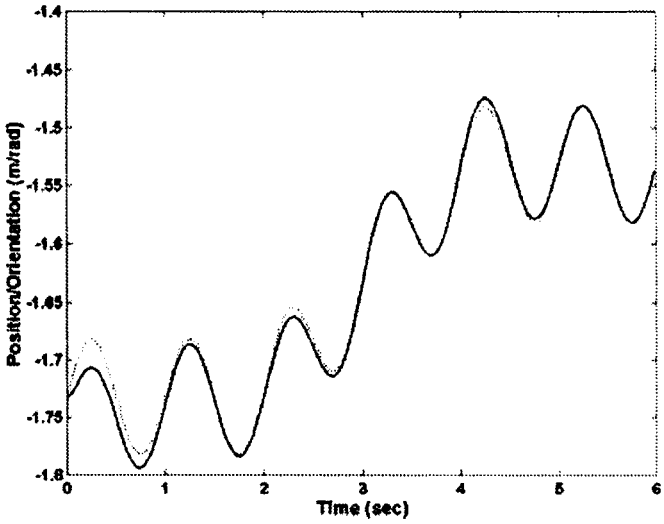

(b) Y-Position Tracking

Fig. 10. Response of object position and orientation for a fixed-base configuration (Egeland-Sagli Problem). The dashed lines indicate desired and the solid lines indicate actual.

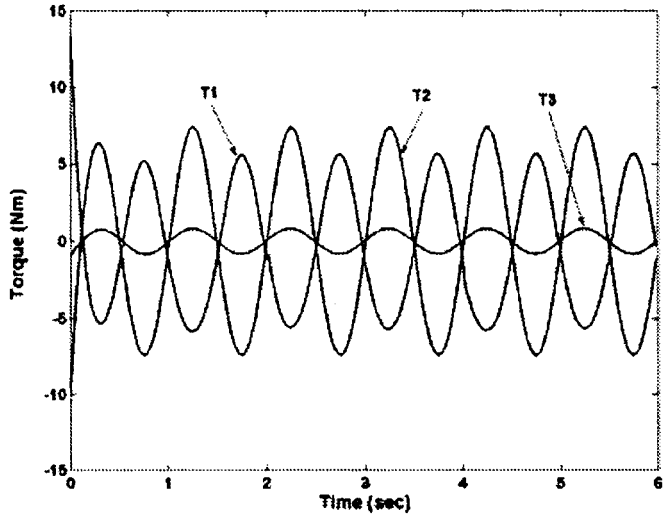

(a) Manipulator 1

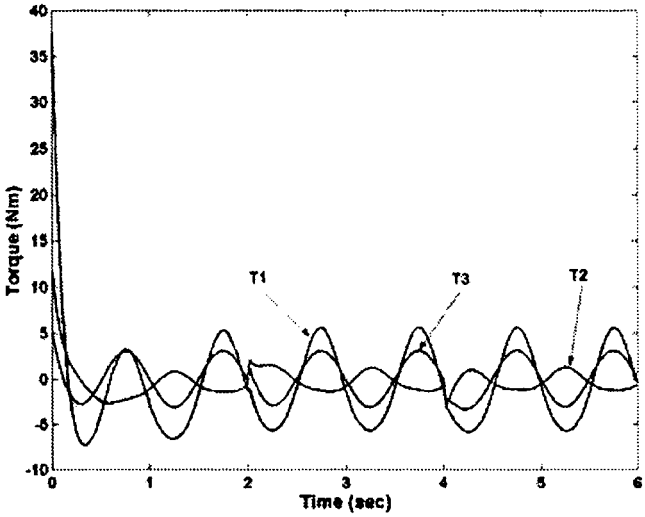

(b) Manipulator 2

Fig. 11. Torque profiles for the fixed-base configuration for the Egeland-Sagli problem.

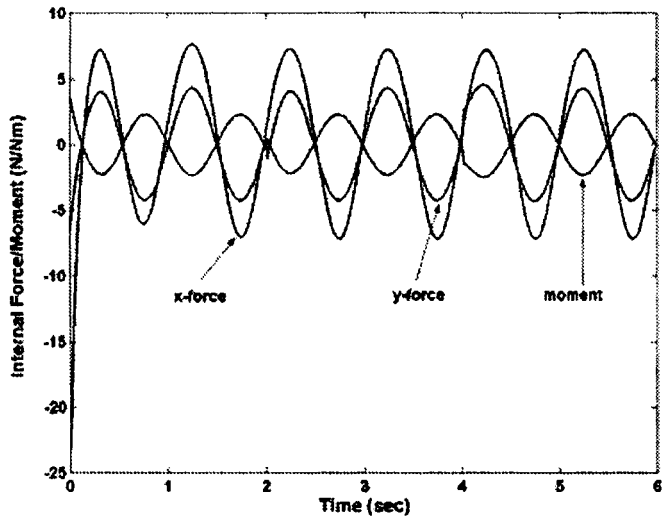

(a) End-effector 1

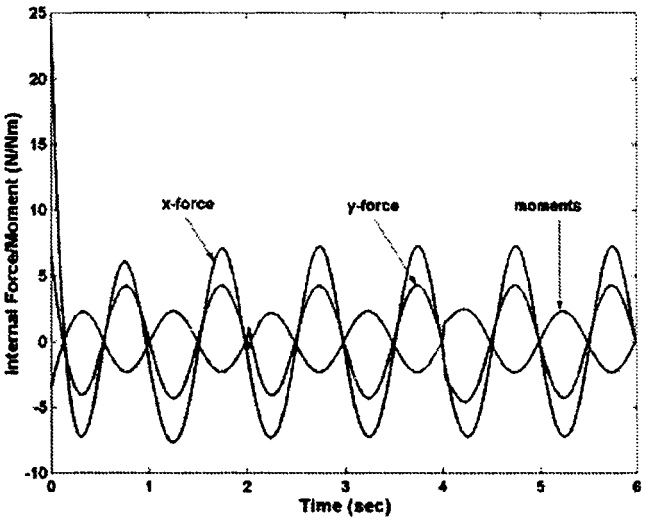

(b) End-effector 2

Fig. 12. Internal forces at the end-effector frames for a fixed-base configuration (Egeland-Sagli Problem).

https://doi.org/10.1017/S0263574703005599 Published online by Cambridge University Press

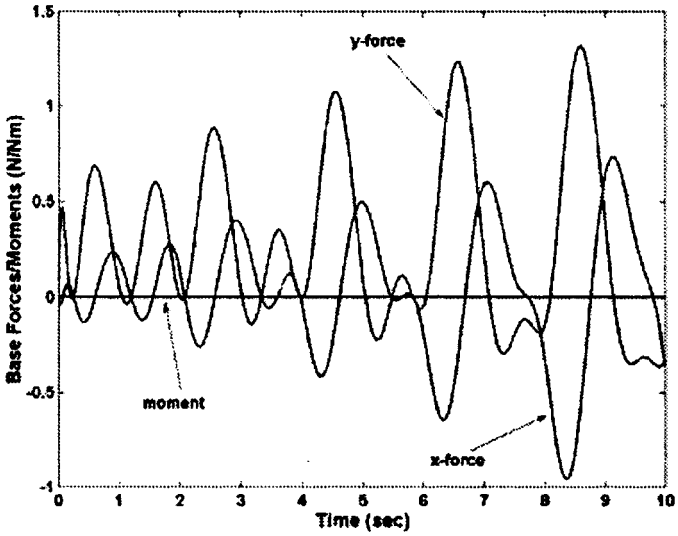

Fig. 13. Base interaction forces in the free-floating configuration with circle problem.

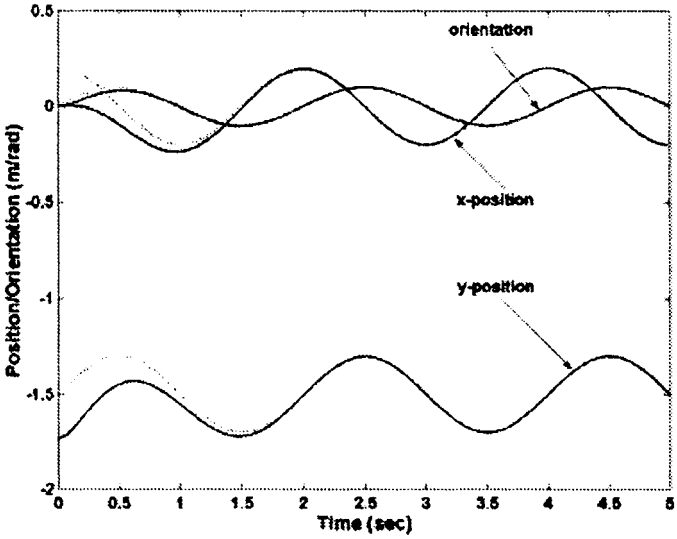

Fig. 15. Position and orientation tracking (Circle Problem). The dashed lines indicate desired and the solid lines indicate actual.

7.3. Free-flying two-arm co-operating manipulator system

For the free-flying, co-operating manipulator system holding an object rigidly whose CM needs to follow desired trajectories, the tracking performance is shown in Figures 15 to 18. The position and orientation tracking performances shown in Figure 15 are the same as in the fixed-base or free-floating system. All the internal forces experienced at the end-effector one are shown in Figure 16. The magnitudes of the internal forces are reasonable. However, the torque requirements shown in Figure 17 and the end-effector forces shown in Figure 18 exhibit excessively higher values. Further, with the progress of time, the magnitudes of the forces and torques increase steadily. Thus, it can be concluded that free-flying systems are not suitable for tracking repeated trajectories. Similar observations are also made for tracking augmented Egeland-Sagli trajectories.

High end-effector forces are needed mostly for maintaining the grip over the object while tracking a desired trajectory in a co-operative manipulator system. These high end-effector forces in turn demand high active joint torques. Further, high frequency oscillations of all the torque and force profiles occurred due to the interaction between the base and the manipulators when counteracted by thruster force to maintain the initial base position. Thus, it is very clear from these studies that the free-flying mode of operation should never be used for co-operating manipulation in space.

8. CONCLUSIONS

In this paper, the tracking control of fixed-base, free-floating, and free-flying co-operating manipulator systems have been presented. In co-operating manipulator systems, closed kinematic chains are formed and, to deal with this situation, the inverse dynamics control algorithms with motive force compensation have been developed for all the three configurations. The performance of the control

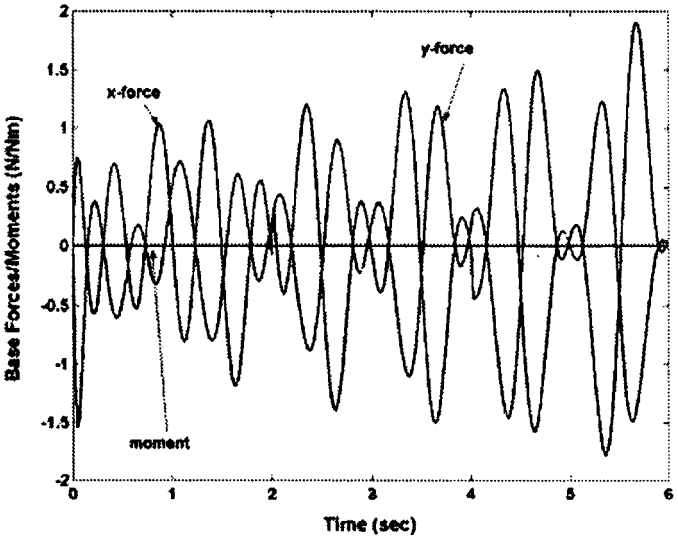

Fig. 14. Base interaction forces in the free-floating configuration with Egeland-Sagli problem.

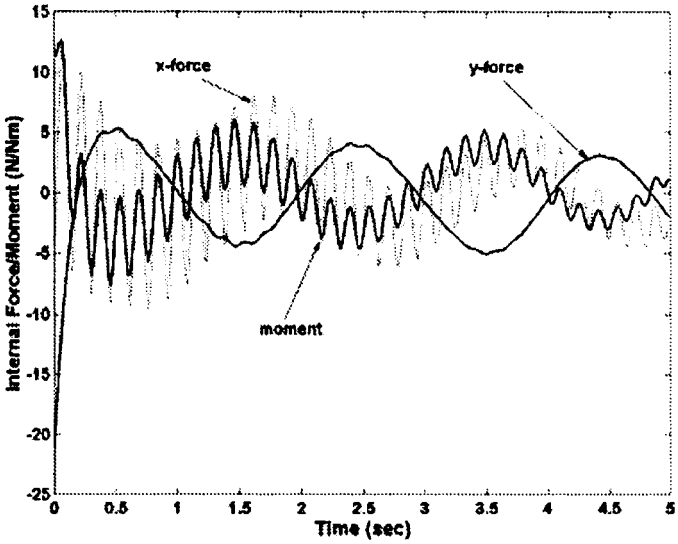

Fig. 16. Internal forces at the end-effector frames for a free-flying configuration (Circle Problem). At End-effector 1.

https://doi.org/10.1017/S0263574703005599 Published online by Cambridge University Press

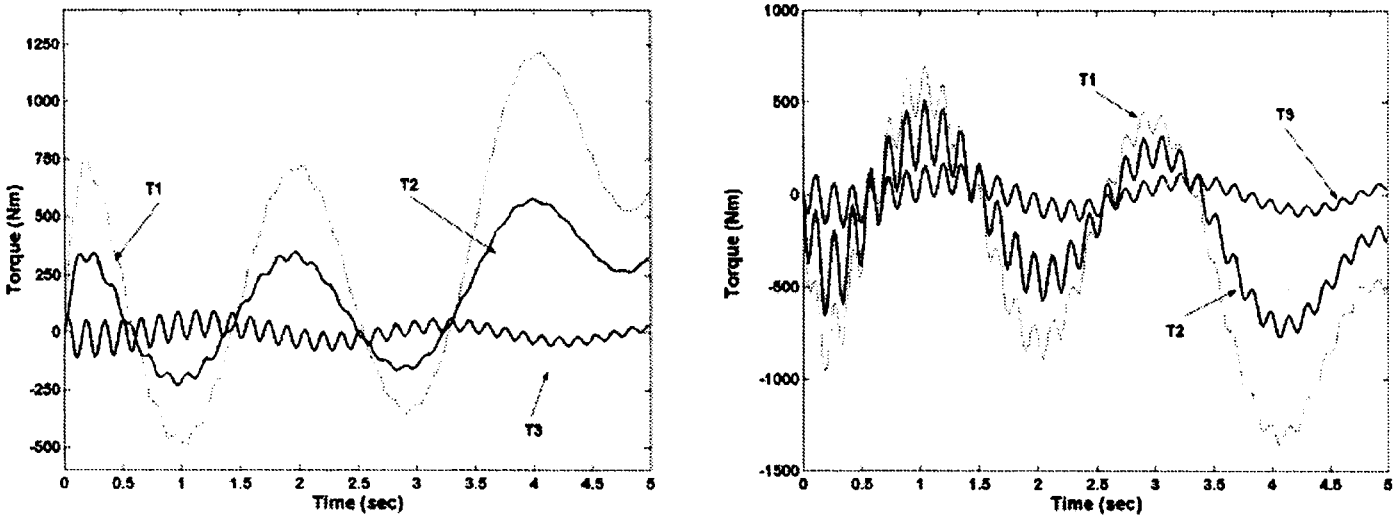

(a) Manipulator 1 (b) Manipulator 2

Fig. 17. Torque profiles for the free-flying configuration for the circle problem.

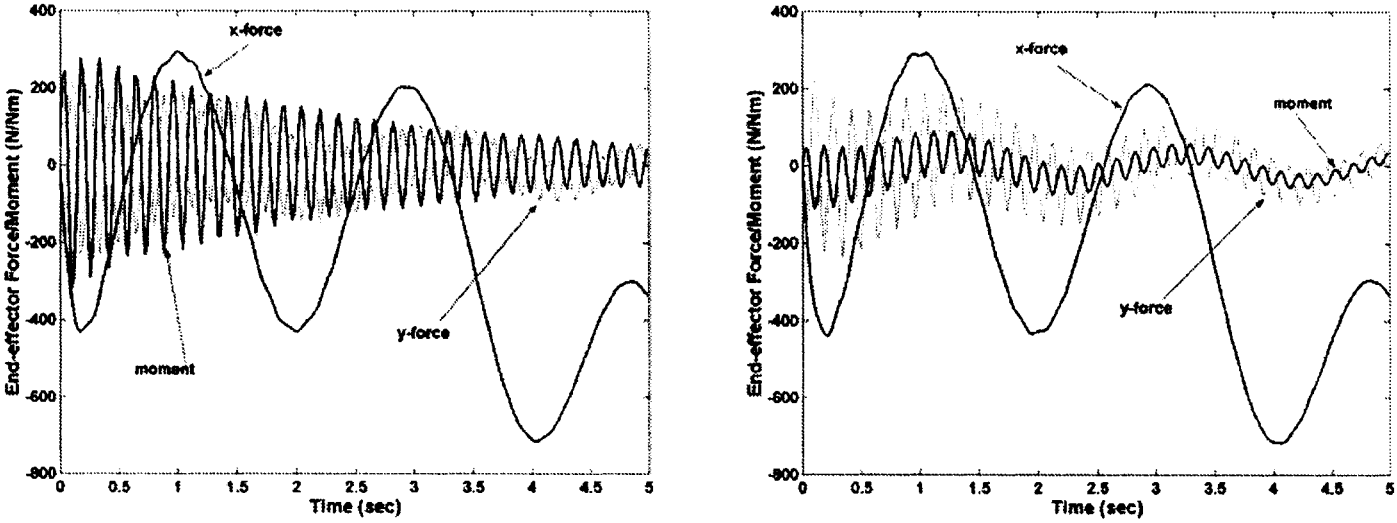

(a) At the End-effector 1 (b) At the End-effector 2

Fig. 18. End-effector forces at the end-effector frames for a free-flying configuration (Circle Problem).

algorithms has been tested for tracking control with the circle and augmented Egeland-Sagli problems.

It has been shown that free-floating space manipulator systems behave in exactly the same manner as that of the fixed-base co-operating manipulator system. The space-free-floating configuration for tracking control required no extra energy to perform the same task as compared to its fixed-base counterpart. Further, it has been shown that, for all space manipulation in the postcapture phase, the free-floating mode is highly advantageous compared to the free-flying configurations. Hence, it has been suggested that the free-floating manipulators should be used for co-operating tasks in space manipulation instead of free-flying manipulators.

References

1. N.H. McClamroch and D. Wang, "Feedback stabilization and tracking of constrained robots," *IEEE Transactions on Automatic Control* **33**, 419–426 (1988).
2. J. Wang, S.J. Dodds and W.N. Bailey, "Co-ordinated control of multiple robotic manipulators handling a common object – Theory and experiments," *IEE Proceedings – Control Theory and Applications* **144**, No. 1, 73–84 (1997).
3. T. Ishida, "Force control in coordination of two amms," *Proceedings of the International Joint Conference on Artifcial Intelligence* (1977) pp. 717–722.
4. C.O. Alford and S.M. Belyeu, "Coordinated control of two robot arms," *Proceedings of the IEEE International Conference on Robotics and Automation* (1984) pp. 468–473.
5. J.Y.S. Luh and Y.F. Zheng, "Constrained relations between two co-ordinated industrial robots for motion control," *Int. J. Robotics Research* **6**, No. 3, 60–70 (1987).
6. S. Arimoto, "Cooperative motion control of multi-robot arms and fingers," *Proceedings of the IEEE International Conference on Robotics and Automation* (1987) pp. 1407–1412.
7. X. Yun, T.J. Tarn and A.K. Bejczy, "Dynamic coordinated control of two robot manipulators," *Proceedings of the IEEE International Conference on Robotics and Automation* (1989) pp. 2476–2481.
8. S. Hayati, "Hybrid position/force control of multi-arm cooperating robots," *Proceedings of the IEEE International Conference on Robotics and Automation* (1986) pp. 82–89.

https://doi.org/10.1017/S0263574703005599 Published online by Cambridge University Press

9. M. Uchiyama and P. Dauchez, "A symmetric hybrid position/force control scheme for the coordination of two robots," *Proceedings of the IEEE International Conference on Robotics and Automation* (1988) pp. 350–356.
10. P. Hsu, "Control of multi-manipulator systems-trajectory tracking, load distribution, internal force control, and decentralised architecture," *Proceedings of the IEEE International Conference on Robotics and Automation* (1989) pp. 1234–1239.
11. P. Hsu, "Coordinated control of multiple manipulator systems," *IEEE Transactions on Robotics and Automation* **9**, No. 4, 400–410 (1993).
12. S.A. Schneider and R.H. Cannon, "Object impedance control for cooperative manipulation: Theory and experimental results," *Proceedings of the IEEE International Conference on Robotics and Automation* (1987) pp. 1076–1083.
13. C.D. Kopf and T. Yabuta, "Experimental comparison of master/slave and hybrid two arm position/force control," *Proceedings of the IEEE International Conference on Robotics and Automation* (1987) pp. 1242–1247.
14. M. Raibert and J. Craig, "Hybrid position/force control of manipulators," *ASME Journal of Dynamic Systems, Measurement and Control* **103**(2), 126–133 (June, 1981).
15. S. Hayati, "Position and force control of coordinated multiple arms", *IEEE Transactions Aerospace Electronics* **24**, No. 5, 584–590 (1988).
16. J. Duffy, "The fallacy of modem hybrid control theory that is based on orthogonal complements of twist and wrench spaces," *Journal of Robotic Systems* **7**, No. 2, 139–144 (1990).
17. M. Vukobratović and R. Stojić, "Historical perspective of hybrid control in robotics: Beginning, evolution, criticism and trends," *Mechanism and Machine Theory* **30**, No. 4, 512–532 (1995).
18. A. Cole, J. Hauser and S. Sastry, "Kinematics and control of multifingered hands with rolling contact," *Proceedings of the IEEE International Conference on Robotics and Automation* (1988) pp. 228–233.
19. A. Cole, P. Hsu and S. Sastry, "Dynamic regrasping by coordinated control of sliding of a multifingered hand," *Proceedings of the IEEE International Conference on Robotics and Automation* (1989) pp. 781–786.
20. G.R. Luecke and K.W. Lai, "A joint error feed-back approach to internal force regulation in cooperative manipulator systems," *Journal of Robotic Systems* **14**, No. 9, 631–648 (1997).
21. J. Wen and K. Kreutz, "Motion and force control for multiple cooperative manipulators," *Proceedings of the IEEE International Conference on Robotics and Automation* (1989) pp. 1246–1251.
22. J. Wen and K. Kreutz, "Motion and force control for multiple robotic manipulators," *Automation* **38**, No. 4, 729–773 (1992).
23. F. Caccavale, P. Chiacchio and S. Chiaverini, "Task-space regulation of cooperative manipulators," *Automatica* **36**, 879–887 (2000).
24. S.H. Murphy, J. T-Y. Wen and G.N. Saridis, "Simulation of cooperating robot manipulators on a mobile platform," *IEEE Transactions on Robotics and Automation* **7**, No. 4, 468–477 (1991).
25. G. Rodriguez, "Recursive forward dynamics for multiple robot arms moving a common task object", *IEEE Transactions on Robotics and Automation* **5**, No. 4, 510–521 (1989).
26. Y. Yokokohji, T. Toyoshima and T. Yoshikawa, "Efficient computational algorithms for trajectory control of free-flying space robots with multiple arms," *IEEE Transactions on Automation* **9**, No. 5, 571–579 (1993).
27. E. Papadopoulos and S. Ali A. Moosavian, "Dynamics and control of space free-flyers with multiple manipulators," *Journal of Advanced Robotics* **9**, No. 6, 603–624 (1995).
28. G.E. Yale and B.N. Agrawal, "Lyapunov controller for cooperative space manipulators", *Journal of Guidance, Control, and Dynamics* **21**, No. 3, 477–484 (1998).
29. Y-R. Hu and G. Vukovich, "Dynamics of free-floating coordinated space robots," *Journal of Robotics Systems* **15**, No. 4, 217–230 (1998).
30. G. Rodriguez, A. Jain and K. Kreutz, "A spatial operator algebra for manipulator modelling and control," *Robotics Research* **10**, 371–381 (1991).
31. G. Rodriguez and K. Kreutz, "Spatial operator factorization and inversion of the manipulator mass matrix," *IEEE Transactions on Robotics and Automation* **8**, No. 1, 65–7 (1992).
32. A. Jain and G. Rodriguez, "An analysis of the kinematics and dynamics of underactuated manipulators," *IEEE Transactions on Robotics and Automation* **9**, No. 4, 411–422 (1993).
33. R. Featherstone, *Robot Dynamics Algorithms* (Kluwer Academic Publishers, USA, 1987).
34. S. Dubowsky and E. Papadopoulos, "The kinematics, dynamics, and control of free-flying and free-floating space robotic systems," *IEEE Transactions on Robotics and Automation* **9**, No. 5, 531–543 (1993).
35. A. Jain and G. Rodriguez, "Base-invariant symmetric dynamics of free-flying manipulators", *IEEE Transactions on Robotics and Automation* **12**, No. 3, 401–405 (1996).
36. S.K. Saha, "A unified approach to space robot kinematics," *IEEE Transactions on Robotics* **12**, No. 3, 401–405 (1996).
37. A.K. Swain, "Dynamic modelling and control of robotic manipulators with an investigation of evolutionary computation methods," *Ph.D. Dissertation* (The University of Sheffield, UK, 2001).
38. P. Chiacchio, S. Chiaverini, L. Sciavicco and B. Siciliano, "Global task space manipulability ellipsoids for multiple-arm systems," *IEEE Transactions on Robotics and Automation* **7**, No. 15, 678–685 (1991).
39. P.C. Hughes, *Spacecraft Attitude Dynamics* (John Wiley: New York, 1986).
40. I.D. Walker, R.A. Freeman and S.I. Marcus, "Analysis of motion and internal loading of objects grasped by multiple cooperating manipulators," *Int. J. Robotics Research* **10**, No. 4, 396–409 (1991).
41. O. Egeland and J.R. Sagli, "Coordination of motion in spacecraft/manipulator system," *Int. J. Robotics Research* **12**, No. 4, 366–379 (1993).

https://doi.org/10.1017/S0263574703005599 Published online by Cambridge University Press